RSC Advances

ROYAL SOCIETY OF CHEMISTRY

www.rsc.org/advances

Journal Name

RSCPublishing

COMMUNICATION

One step synthesis of zinc oxide containing boron nitride carbon sheets for oxygen reduction reaction and degradation of organic dye

Cite this: DOI: 10.1039/x0xx00000x

A. Yamuna, Aditya Mandalam, R. Karthigaiselvi, M. Balasubramanian, B. Thiruparasakthi, Subbiah Ravichandran and Sundar Mayavan*

Received 00th January 2012,
Accepted 00th January 2012

DOI: 10.1039/x0xx00000x

www.rsc.org/

In this work, zinc oxide containing boron nitride carbon sheets (ZnO/h-BNC) with hexagonal B-N bond structure was prepared using a scalable, one-step process involving the thermal treatment of glycine, zinc nitrate, graphene oxide and boron oxide. The as-prepared ZnO/h-BNC hybrids were found to be active for both electrocatalytic reduction of oxygen in alkali condition and photocatalytic oxidation of dye, respectively. The ZnO/h-BNC showed much improved onset potential and reduction current density, compared with ZnO/BCN sheets with C=N dominant bond configuration for ORR. The BNC riched with h-BN shows excellent ORR performance, while C=N dominant BCN shows relatively less activity for ORR, suggesting the intrinsic properties differences of BCN based materials with different bond configurations. The Zn species located inside h-BNC matrix act as photocatalytically active centres for degradation of methyl orange dye under UV irradiation.

Synthesis of advanced functional materials is essential to address much of our present energy and environmental related concerns and steer us to a bright green future. The advent of graphene with its exciting electronic, mechanical and chemical properties has changed the landscape of materials research.[1,2] The rise of graphene saw the emergence of structurally similar material such as hexagonal boron nitride (h-BN) and carbon nitride (CN), a wide band gap semiconductor with high thermal conductivity and strong luminescence in UV range.[3,4] Recently, Boron (B), nitrogen (N) and carbon (C) containing two dimensional nano sheets have shown tremendous potential in applications ranging from electronics to catalysis.[5-7] Carbon (C) and oxygen (O) doping within layered h-BN structures were found to modify the adsorption and light emission properties. For example, D. Portehault et al.[8] reported high surface area boron carbon nitrides (BCN) exhibiting excellent hydrogen uptake properties. W. Lei et al.[9] reported boron carbon nitride nanostructures exhibiting tunable water-soluble phosphors. BCN has been synthesized in various forms. Y. Zheng et al[10] prepared g-BCN structures with B and N homogenously doped in graphene lattice and h-BCN structures with graphene embedded h-BN networks. But with respect to performance and property these two kinds of BCN structures are strikingly different with g-BCN and h-BCN behaving more like doped graphene and doped h-BN, respectively.[10,11] The bonding configuration between B, N and C largely determines their physical, chemical, catalytic and electronic properties and it remains a challenge to control their bond structure by a facile and convenient manner.

Previous methods towards synthesis of BCN nanomaterial mainly involve multistep process and CVD method. Hence, it is necessary to explore new and simpler methods to develop BCN based compounds. In fact, BCN sheets have been successfully synthesized by annealing urea (as a N source), boric acid (as a B source) and PEG[12] or activated carbon[13] (as a C source). Here, for the first time, we developed a synthetic protocol for the synthesis of zinc oxide containing h-BNC nanosheets via glycine-nitrate chemistry and its activity towards catalysing oxygen reduction reaction and dye degradation. The new catalyst (ZnO/h-BNC) that consist predominantly of domains of h-BN and carbon shows excellent activity in the ORR and perfect (nearly 100%) selectivity for the four-electron ORR pathway in an alkaline medium as compared to BCN structures with C=N and h-BN domains. The current study on BCN structures may provide new insight into the, structure-property relationship and feasible synthesis of more advanced catalysts for potential applications

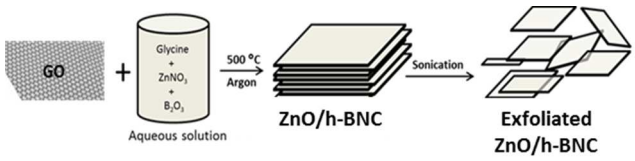

Scheme1. Schematic illustration of the synthesis procedure of ZnO/h-BNC nanosheets

in fuel cells and metal–air batteries. The glycine-nitrate chemistry previously described for the synthesis of ceramic oxides[14] was adapted to prepare ZnO/h-BNC nanosheets. Glycine was used to reduce nitrate ions, resulting in the decomposition of a glycine-nitrate mixture beyond 200ºC.[14] The products of decomposition (NOx, COx, etc,.) along with B_2O_3 and graphene oxide (GO) act as precursor for the synthesis of ZnO/h-BNC. In brief, Glycine (Gly), Zinc nitrate ($ZnNO_3$), GO (Figure S1) and boron oxide (B_2O_3) was added together in water, followed by sonication to form a homogenous aqueous solution. The aqueous mixture was then transferred to tubular furnace and heated at 500° C for 2 h under argon flow to form ZnO/h-BNC sheets (see scheme 1 and experimental in supporting information).

XPS measurements were performed to determine the surface electronic state of the ZnO/h-BNC. In order to understand the formation of ZnO/h-BNC, the XPS spectra of GO-Gly-$ZnNO_3$-B_2O_3 annealed at two different temperatures (at 300 and 500 ºC) was analysed. Figure 1a shows the B 1s spectra at two different temperatures. At 300° C, B 1s spectra show major peak at around 197 eV which corresponding to B-O band.[15] As the temperature increased to 500 °C, these peaks disappeared, and a new major peak at 191.6 eV was observed, which is close to that of B 1s in h-BN.[16] This suggests that the main bonding configuration for B in our films is similar to that of h-BN. At 300° C, the N1 s (Figure 1b) spectra show major peak at around 404 eV which corresponding to N-O species. But this peak disappeared at 500 °C and a new peak showed up at 398.6 eV which is similar to the position of N 1s spectrum of h-BN.[16]. Both the B 1s and the N 1s spectrum indicate that the main configuration for B and N atoms is the B-N bond, implying that h-BN domains exist in the film. At 300° C, the high resolution C 1s XPS spectra (Figure 1c) show a major peak at around 290 eV which corresponding to carbon atoms attached to different oxygen-containing moieties.[17] XPS C1s spectra at 500 ºC (in Figure 1c) clearly show an almost total loss of the oxygen component above 286 eV, while C=C bond at 284.5 eV dominate, which is close to the value observed in graphite (284.9 eV). This suggests that the C-C bonds stay together and form graphene domains. A small shoulder toward the low binding energy side at around 282 eV suggested the presence of carbon atoms in carbide form, indicating the substitution of carbon for oxygen and the formation of Zn-C bonds as in case of carbon-doped ZnO nanostructures.[18,19] At 300°C (Figure S5, supporting information), the O1s spectrum show peak at 537.2 eV which corresponding to NO_2 oxygen.[20] As the annealing temperature was increased to 500° C, these peaks disappeared, suggesting the removal of NO_2 oxygen and a new broad peak showed up at around 531.6 eV with a shoulder at 528.4 eV, suggesting the O1 s components locates in different environment. The peak at 531.6 may be ascribed to surface adsorbed oxygen species. The peak at 528.4 eV is assigned to O^{2-} ions of Zn–O bonds in wurtzite structure with Zn^{2+} in hexagonal coordination.[18] A typical XPS spectrum (Fig. 1d) at 300 ºC revealed a $Zn2p_{3/2}$ binding-energy (BE) peak at 1027 eV and 1050 eV. But at 500° C, the Zn 2p core-level XPS spectrum (Figure 1d) shows doublet spectral lines at binding energies of 1020.5 eV Zn2p3/2 and 1043.6 eV Zn 2p1/2 with a spin-orbit splitting (1E) of 23.2 eV, which is close to value of 1021.6 eV and 1044.7 eV measured for zinc (II) oxide.[18,19] Thus the resulting material consists of predominantly B-N and carbon domains. From this XPS data, it is evident that the annealing temperatures of 500 ºC were sufficient to remove and dissociate oxygen, NOx and other intermediate products toward formation of ZnO/h-BNC structures.

Information about bonding structure has been probed by IR spectroscopy. Pure hexagonal BN presents two characteristic absorption bands at 1375 and 750 cm^{-1} associated with the in-plane stretching and the out-of-plane bending vibration,

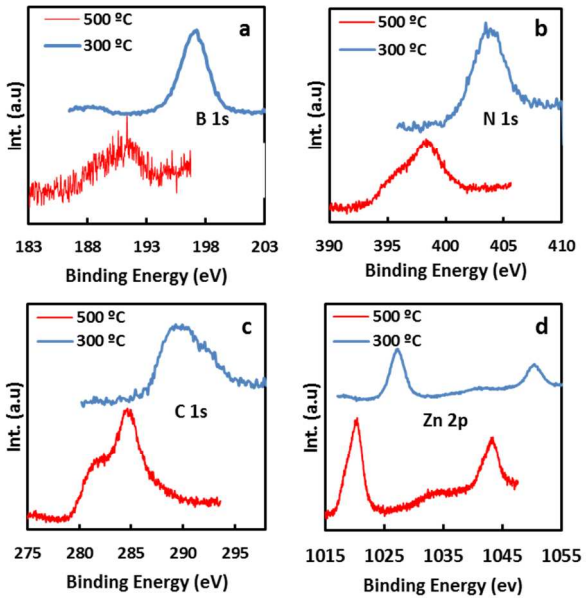

Figure 1. High-resolution (a) XPS B 1s, (b) N 1s, (c) C 1s and (d) Zn 2p of ZnO/h-BNC at 300 and 500 ºC

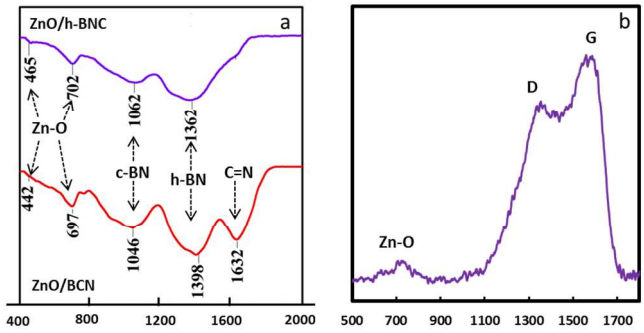

Figure 2.(a) FTIR spectra of ZnO/h-BNC and ZnO/BCN; (b) Raman spectra of ZnO/h-BNC

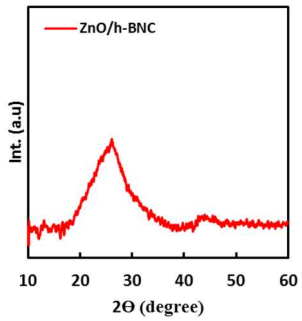

Figure 3. XRD pattern of ZnO/h-BNC

respectively.[21] Figure 2 a show the IR spectra of h-BNC structures. h-BNC structures show absorption bands at 1352 cm^{-1} and out of phase bending vibration around 750 cm^{-1} is hardly detected for this material. These results confirm the amorphous nature of the layer and the predominant hexagonal structure.[22] With regards to main B-N band, there is a shift from 1370 to 1352 cm^{-1} for h-BNC. Such a change suggests compositional changes within the basal planes, i.e. B-N-C intermixing.[22] In addition to h-BN, c-BN phases are also formed. It is interesting to note that BCN structures prepared under similar experimental conditions without GO show bands characteristic for h-BN, B-C and C=N phases. These results suggest that GO inclusion (in the synthesis) favours the formation of h-BN rich carbon domains without C=N phase. In addition, both the above structures (h-BNC and BCN) shows prominent Zn-O bond. The Raman spectra of ZnO/h-BNC exhibit two broad amorphous peaks, corresponding to D band (at 1355 cm^{-1}) and G (at 1581 cm^{-1}) band,[10] along Zn-O band at 743 cm^{-1}.

The (002) diffraction peak for h-BN and graphite are reported at 2Θ = 26.8° (d = 3.42 Å) and at 2Θ = 26.6° (d = 3.36 Å), respectively and with increase in carbon content the reflection varies from 25.0° to 26.3°.[23] Therefore, the broad XRD peak observed at 26.2º (002) and 42.3º (100) for as-prepared ZnO/h-BCN sample (Figure 3) indicates formation of amorphous h-BNC structure with high carbon content. Interestingly, the XRD pattern of ZnO/h-BNC does not show any peak originating from zinc species, such as zinc oxide, zinc, zinc nitride, and zinc carbides. However, $ZnNO_3$ heated under similar conditions shows characteristic ZnO crystallite peaks. The non-observance of Zn peaks for as-prepared sample is an indication that zinc species are chemically coordinated to the h-BNC host. XPS data suggests Zn-C and Zn-N bond formation. Similar type of coordinated structures (with clear absence of XRD peaks) was reported by S. Wang et al[24] and Q. Liu et al[25] in iron and cobalt containing carbon nitrides compounds. But exact nature of bonding is not known and further work is needed to determine the local structure of zinc species. Finally, the morphology of as-prepared ZnO/h-BNC was analysed by field emission scanning electron microscopy (FE-SEM) and transmission electron microscopy (TEM). FE-SEM image (Figure 4 a-b) indicates the formation of macro porous sheets stacked together. The elemental mapping (Figure S2) reveals that B, C, N, O and Zn species are homogeneously distributed and we can conclude that h-BNC possess a consistent B-N-C structure. Sonication was used as a top down method to exfoliate stacked sheets. The exfoliation process involves cutting or direct peeling off from the as-prepared product. TEM was used to investigate the microscopic structure of sonicated h-BNC. As displayed in Figure 4 c-d, the h-BNC shows crumbled and aggregated nanosheets morphology.

The electrocatalytic behaviours and activity of as-prepared ZnO/h-BNC and ZnO/BCN for ORR (in 0.1M KOH solution saturated with oxygen) are examined by cyclic voltammetry (CV) and the current density presented here equals the measured

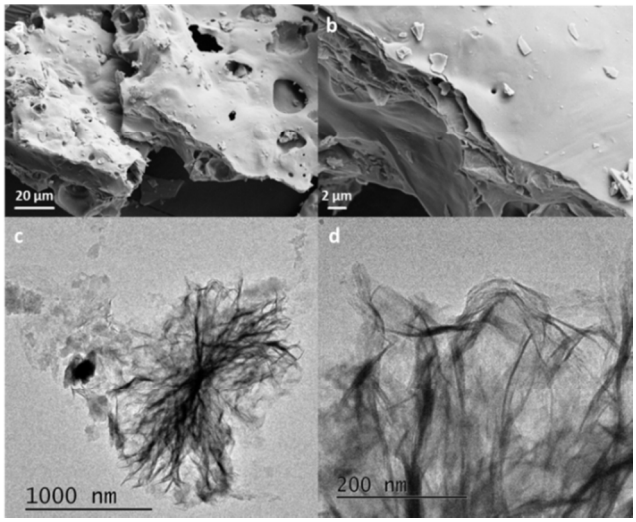

Figure 4. FE-SEM and TEM images of ZnO/h-BNC at different magnification

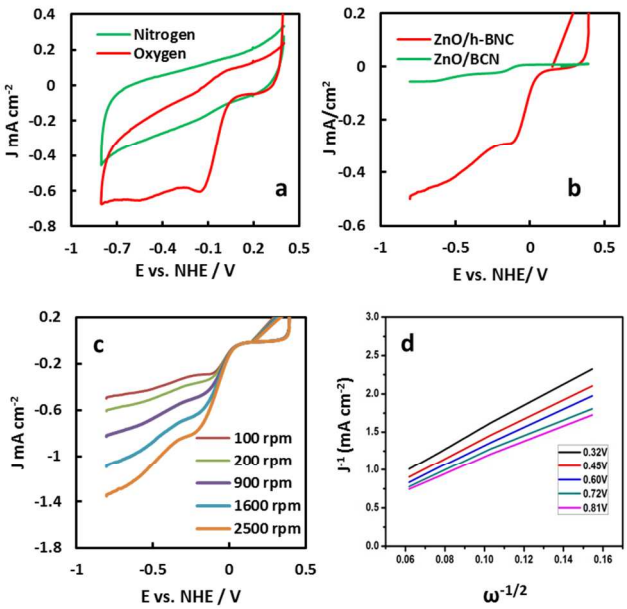

Figure 5. (a) Cyclic voltammograms of ZnO/h-BNC at a scan rate of 50 mVs^{-1} in O_2 and N_2-saturated 0.1m KOH solution. (b) RDE LSC voltammograms of ZnO/h-BNC and ZnO/BCN nanosheets at a rotation rate of 100 rpm. (c) Rotating disk electrode (RDE) linear sweep voltammograms of ZnO/h-BNC in O_2-saturated 0.1m KOH with various rotation rates at a scan rate of 10 mVs^{-1}. (d) Koutecky–Levich plots of J −1 vs. ω−1/2 at different potentials derived from the RDE measurements

current divided by the geometric surface area of the GC electrode. As shown in Figure 5 a, featureless voltammetric currents within the potential range from -0.8 to +0.4 V are observed for ZnO/h-BNC in the nitrogen saturated solution. In contrast, a well-defined cathodic peak centered at -0.30 V (vs. SCE) emerges in CV as the electrolyte solution is saturated with oxygen, hence suggesting a pronounced electrocatalytic activity of as-prepared BCN-G for oxygen reduction. To further evaluate the electrocatalytic activity of ZnO/h-BNC, linear-sweep voltammetry (LSV) of ZnO/h-BNC and ZnO/BCN sheets at a rotation speed of 100 rpm was also measured in the O_2-saturated 0.1 mol/L KOH solution on RDE, as seen in Figure 5b. Clearly, the ZnO/h-BNC exhibit much higher current density compared with the ZnO/BCN catalyst and the value of limiting reduction current density (J) at -0.75 V vs. NHE for ZnO/h-BNC is eight times higher than that of pristine ZnO/BCN, indicating a greatly enhanced activity for ORR by the introduction of graphene. It is striking that the onset potential of ZnO/h-BNC nanosheets (-0.30 V) is more positive than those of ZnO/BCN nanosheets and only 95 mV (vs. SCE) higher than the reported commercial Pt/C catalyst. This over potential difference of 95 mV for ZnO/h-BNC w.r.t Pt/C is lesser than reported N-graphene (200 mV vs SCE),[26] B-Nanotube (150 mV vs. SCE),[27] Nanoporous graphitic-C_3N_4@Carbon (100 mV vs. SCE).[28] The potential of oxygen reduction for as-prepared ZnO/h-BNC was compared with ZnO/BCN. The half-wave potential, a potential at which the current is a half of the limiting current in a LSV curve, has been used for this purpose. It is interesting to see from Figure 4b that the half-wave potential of the ZnO/h-BNC electrode for ORR in 0.1m KOH solution was at around -0.2 V vs SCE, which is much more positive than pristine ZnO/BCN (-0.35 V).

Furthermore, a set of LSV curves for ORR based on the ZnO/h-BNC catalyst recorded from 100 to 2400 rpm was shown in Figure 5c. The result shows that as the rotation speed increases, the measured ORR current also increases. This is due to the decrease in diffusion layer thickness with increase in rotation rate and more oxygen molecule will get reduced at the electrode surface. The koutecky-levich (K-L) plots were obtained from the polarization curves at different potentials, as seen in Figure 5d. The K-L plot showed good linearity and near parallelism over the potential range of -0.32 V to -0.81 V, which suggest first order reaction kinetics and similar electron transfer number at different potentials. The number of electron transfer (n) for ZnO/h-BNC is found to be 3.6, 3.8, 3.87, 3.88, 3.92 at 0.32 V,0.45 V, 0.60 V, 0.72 V, 0.81 V respectively which suggests that the ZnO/h-BNC catalyst exhibit dominant four electron ORR process.

To further evaluate the properties of as-prepared ZnO/h-BNC as potential electrocatalyst, the crossover effect should be considered because the fuel molecules such as methanol in the anode sometimes permeate through the polymer membrane to the cathode and seriously affect the performance of the cathode catalysts.[29] Thus, the electrocatalytic sensitivity of ZnO/h-BNC and commercial Pt-C catalysts were measured against the electro oxidation of methanol in ORR. A strong response is observed for the Pt-C catalyst in O_2-saturated 0.1M KOH solution with 1M methanol,[26] whereas no noticeable response for ZnO/h-BNC is detected under the same testing conditions. This shows that as-prepared ZnO/h-BNC nanosheets exhibit high selectivity for ORR with a remarkably good tolerance of crossover effects, thus being superior to the commercial Pt-C. Since the ZnO/h-BNC nanosheets and their counterparts (ZnO/BCN nanosheets) obtained by the same synthesis procedure without GO inclusion, the significantly enhanced activity of the ZnO/h-BNC nanosheets must be attributed to the formation of hB-N dominant graphene domains, as compared to B-N and C=N dominant BCN sheets in case of BCN sheets prepared without GO. This suggests the importance of bonding configuration between B, N and C that largely determines their catalytic activity for ORR.

The presence of ZnO in the ZnO/h-BNC allowed us to evaluate its effectiveness for photocatalysis. ZnO/h-BNC sample was tested for degradation of dye at room temperature under UV light. Figure 6a shows the photocatalytic activities of the sample under UV light. Blank experiment was performed with MO dye in water under same conditions but without any catalyst to exclude a possible photolysis of the dye UV light. No or very low MO degradation was observed in the absence of ZnO and ZnO/h-BNC. Only 22% of MO can be degraded by pure ZnO (control) in 2 h. The use of ZnO/h-BNC sheets leads to 83 % photo degradation of MO in about 30 min. MO dye exhibits a characteristic absorption peak at 473 nm.[30] Figure 6 b demonstrated that the degradation of MO dye (quenching of MO absorbance peak by 83%) and a decrease in colour compared with original solution was clearly observed. These results clearly demonstrate that the ZnO/h-BNC exhibit excellent photo catalytic activity as compared to pristine ZnO. The electronic interaction between ZnO and ZnO/h-BNC (acts as an electron sink) plays a vital role for the efficiency of separation of generated charges (e-h pairs).[31,32] This charge separation process effectively reduces the chances of the recombination of newly generated electrons and holes, therefore significantly increasing the lifetime of holes in ZnO/h-BNC as compared to ZnO. These accumulated holes with longer lifetime can either react with adsorbed water to form hydroxyl radicals or directly oxidize various organic compounds, inducing the faster photo degradation as reported by several authors.

The photoinduced electron–hole pair recombination kinetics is considered to be a most important factor that affects the photocatalytic efficiency of a photocatalyst.[33] The electron hole

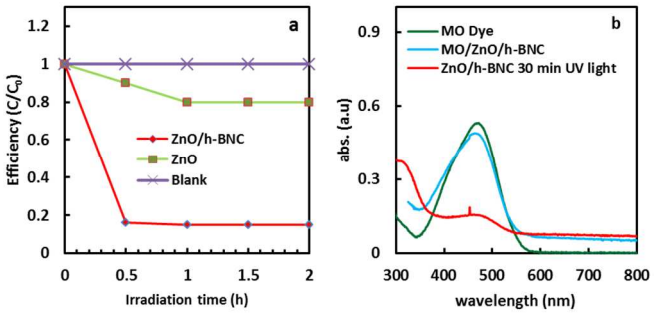

Figure 6. (a) Degradation rate of MO under UV light irradiation in the presence of ZnO/h-BNC, ZnO and blank; (b) Degradation process of MO dye in presence of ZnO/h-BNC under UV light.

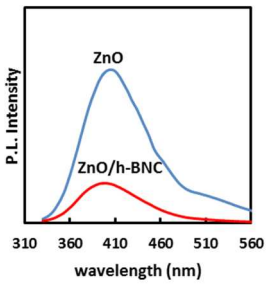

Figure 7. Photoluminescence (PL) spectra of ZnO and ZnO/h-BNC

pair recombination efficiency can be experimentally determined by PL emission spectra. A lower PL emission intensity indicates the better charge separation efficiency.[31] In Figure 7, the strong UV peak at around 400 nm was observed for ZnO due to its free excitonic emission near the band edge. For comparison, chemically bonded ZnO/h-BNC was analysed with PL emission spectra. The emission intensity decreased largely, suggesting that the bonding with ZnO/h-BNC could quench the fluorescence from ZnO. The quenching mechanism of the PL spectra may be because of the interfacial charge transfers from the excited semiconductor nanoparticles. It may be possible to increase the rate of charge transfer, and thus the interfacial interaction between the semiconductors and h-BNC. Therefore, h-BNC is a promising candidate for enhancing the photocatalytic activity in terms of prolonging the electron–hole pair lifetime, which inhibits the recombination and accelerates the interfacial charge transfer process.

In conclusion, we have demonstrated a single step method toward synthesis of metal oxide containing h-BNC nanosheets by thermal treatment of glycine, $ZnNO_3$, GO and B_2O_3 at 500° C. The compound riched with h-BN shows excellent ORR activity in alkaline solution, while BCN compounds with B-N and C=N shows less activity for ORR. This method provides not only an effective approach for fabricating ZnO/h-BNC that is cheap yet of high quality but also a new concept to control the B, C and N bonding configurations in BCN. In addition, ZnO/h-BNC is also phocatalytically active for dye degradation and shows much better activity than pristine ZnO. More importantly, by using our approach it is possible to synthesis a series of h-BNC based materials containing semiconductor or nanoparticles in a single step process for variety of applications like sensors, super capacitors, and lithium batteries.

Notes and references

CSIR-Central Electrochemical Research Institute, Karaikudi, India
914565241453; sundarmayavan@cecri.res.in

† Electronic Supplementary Information (ESI) available: Experimental, instrumentation, AFM image of GO and Elemental mapping of ZnO/h-BNC. See DOI: 10.1039/c000000x/

1. A. Thomas, A. Fischer, F. Goettmann, M. Antonietti, J-O Muller, R. Schlogl and J. M. Carlsson *J. Mater. Chem*., 2008, **18**, 4893
2. N. Zhang, Y. Zhang and Y-J Xu, *Nanoscale*, 2012, **4**, 5792
3. Y. Zheng, J. Liu, J. Liang, M. Jaroniec and S. Zhang Qiao, *Energy Environ. Sci*., 2012, **5**, 6717
4. Y. Sun, Q. Wu and G. Shi, *Energy Environ. Sci*., 2011,**4**, 1113
5. H. Wang, C. Zhang, Z. Liu, L. Wang, P. Han, H. Xu, K. Zhang, S. Dong, J. Yao, G. Cui, *J. Mater. Chem*., 2011, **21**, 5430.
6 L. Qu, Y. Liu, J. B. Baek and L. Dai, *ACS Nano*, 2010, **4**, 1321.
7 Y. Wang, Y. Shao, D. W. Matson, J. Li, Y. Lin, *ACS Nano,* 2010, **4**, 1790
8. Q. Liu and J. Zhang, *Langmuir,* 2013, **29**, 3821
9. W. Lei, D. Portehault, R.Dimova and M. Antoniett, *J. Am. Chem. Soc*., 2011, **133,** 5660
10. Y. Zheng, Y. Jiao, L. Ge, M. Jaroniec, S. Z. Qiao, *Angew. Chem., Int. Ed*. 2013, **125**, 3110.
11. O. Stephan, P. M. Ajayan, C. Colliex, P. Redlich, J. M. Lambert, P. Bernier, P. Lefin, *Science*, 1994, **266**, 1683
12. K. Raidongia, A. Nag, K. Hembram, U. V. Waghmare, R. Datta and C. N. R. Rao, *Chem.;Eur. J.* 2010, **16**, 149.
13. J. Jin, F. Pan, L. Jiang, X. Fu, A. Liang, Z. Wei, J. Zhang and G. Sun, *ACS Nano*, 2014, **8**, 3313.
14. C. Toniolo, M.D. Lima, A.S. Takimi, C.P. Bergmann. *Mat. Res. Bull.,* 2005, **40**, 561
15. K. Jayaramulu, N. Kumar, A. Hazra, T. K. Maji and C. N. R. Rao, *Chem. Eur. J.* 2013, 19, 6966
16. L. Ci, L. Song, C. Jin, D. Jariwala, D. Wu, Y. Li, A. Srivastava, Z. F.Wang, K. Storr, L.Balicas, F. Liu and P. M. Ajayan, *Nature Mater*. 2010, **9**, 430
17. V. Datsyuka, M. Kalyva, K. Papagelis, J. Parthenios, D. Tasis,A. Siokou, I. Kallitsis, C. Galiotis, *Carbon*, 2008, **46**, 833
18. A S. Alshammari, L. Chi, X. Chen, A. Bagabas, D. Kramer, A. Alromaeha and Z. Jiang, *RSC Adv*., 2015, **5**, 27690
19. J. W. Park, D. H. Kim, S-H Choi, M. Lee and D. Lim, *J Korean Phy Soc.* 2010, **57**, 1482.
20. A. Krepelova, J. Newberg, T. Huthwelker, H. Bluhm and M. Ammann, *Phys. Chem. Chem. Phys*., 2010, **12**, 8870
21. Y.Wada, Y.K. Yap, M. Yoshimura, Y. Mori, T. Sasaki, *Diamond Relat. Mater*., 2000, **9**, 620
22. I. Caretti , J.M. Albella, I. Jiménez, *Diamond Relat. Mater.,* 2007, 16, 63.
23. R. Torres, I. Caretti R. Gago, Z. Martín, I. Jiménez, *Diamond Relat. Mater.,* 2007, 16, 1450.
24. X. Wang, X. Chen, A. Thomas, X. Fu, M. Antonietti, *Adv. Mater.* 2009, **21**, 1609.
25. Q.Liu and J. Zhang. *Langmuir* 2013, **29**, 3821
26. Z. Luo, S. Lim, Z. Tian, J. Shang, L. Lai, B. MacDonald, C. Fu, Z. Shen, T. Yu, J. Lin, *J. Mater. Chem*., 2011, **21**, 8038
27. L. Yang, S.J iang, Y. Zhao, L. Zhu, S. Chen, X. Wang, Q.Wu, J. Ma, Y. Ma, Z. Hu, Z, *Angew. Chem. Int. Ed,* 2011, **50**, 7132.
28. Y. Zheng, Y. Jiao, Y. Chen, J. Liu, J. Liang, A. Du, W. Zhang, Z. Zhu, S. C. Smith, M. Jaroniec, G. Qing, S. Z. Qiao*., J.Am.Chem.Soc*, 2011, **133**, 20116.
29. L. T. Qu, Y. Liu, J. B. Baek, L. M. Dai, *ACS Nano* 2010**, 4**,1321
30. A. Ye, W. Fan, Q. Zhang, W. Deng and Y. Wang, *Catal. Sci.Technol*., 2012, **2**, 969
31. N. Zhang, Y. Zhang and Y-J Xu, *Nanoscale,* 2012, **4**, 5792
32. X. Zhou, B. Jin, L. Li, F. Peng, H. Wang, H. Yu and Y. Fang, *J. Mater. Chem*., 2012, **22**, 17900
33. N. Cheng, J. Tian, Q. Liu, C. Ge, A. H. Qusti, A. M. Asiri, A O. Al-Youbi and X. Sun, *ACS Appl. Mater. Interfaces,* 2013, **5**, 6815